J Nanopart Res (2012) 14:1139
DOI 10.1007/s11051-012-1139-3

RESEARCH PAPER

UV-induced photochemical transformations of citrate-capped silver nanoparticle suspensions

Justin M. Gorham · Robert I. MacCuspie · Kate L. Klein · D. Howard Fairbrother · R. David Holbrook

Received: 27 June 2012 / Accepted: 17 August 2012 / Published online: 14 September 2012

Abstract Due to the increasing use of silver nanoparticles (AgNPs) in consumer products, it is essential to understand how variables, such as light exposure, may change the physical and chemical characteristics of AgNP suspensions. To this end, the effect of 300 nm ultraviolet (UV) light on (20, 40, 60 and 80) nm citrate-capped AgNP suspensions has been investigated. As a consequence of irradiation, the initial yellow hue of the AgNP suspensions is transformed towards a near colorless solution due to the loss of the surface plasmon resonance (SPR) absorbance. The decrease in SPR absorbance followed a first-order decay process for all particle sizes with a rate constant that increased linearly with the AgNP specific surface area and non-linearly with light intensity. The rate of loss of the SPR absorbance decreased with increasing citrate concentration, suggesting a surface-mediated transformation. Absorbance, atomic force microscopy, and dynamic light scattering results all indicated that AgNP photolysis was accompanied by a diameter decrease and occasional aggregation. Furthermore, in situ transmission electron microscopy imaging using a specialized liquid cell also showed a decrease in the particle size and the formation of a core–shell structure in UV-exposed AgNPs. X-ray photoelectron spectroscopy analysis suggested that this shell consisted of oxidized silver. The SPR in UV-exposed AgNP suspensions could be regenerated by addition of a strong reducing agent ($NaBH_4$), supporting the idea that oxidized silver is present after photolysis. Evidence for UV-enhanced dissolution and the production of silver ions was obtained with the Donnan membrane technique. This study reveals that the physico-chemical properties of aqueous AgNP suspensions will change significantly upon exposure to UV light, with implications for environmental health and safety risk assessments.

Keywords Silver nanoparticles · AgNPs · Photolysis · NanoEHS · Nanoparticle transformations · Liquid TEM

Electronic supplementary material The online version of this article (doi:10.1007/s11051-012-1139-3) contains supplementary material, which is available to authorized users.

J. M. Gorham (✉) · R. I. MacCuspie · K. L. Klein · R. D. Holbrook
Material Measurement Laboratory, National Institute of Standards and Technology, Gaithersburg, MD 20899, USA
e-mail: justin.gorham@nist.gov

D. H. Fairbrother
Department of Chemistry, Johns Hopkins University, Baltimore, MD 21218, USA

Introduction

The rising use of silver nanoparticles (AgNPs) in consumer products has heightened concerns over the potential risk that AgNPs could pose upon reaching the environment (Rai et al. 2009; Maynard 2010; Tolaymat et al. 2010), attracting attention and debate

from the public, researchers, and regulators (Nowack 2010; Costanza et al. 2011; Nowack et al. 2011a, b). For AgNPs these nano-related environmental, health, and safety (nanoEHS) concerns (Wiesner et al. 2009; Tolaymat et al. 2010) can be broadly grouped into three interrelated categories: (I) release from products; (II) transformation, fate and transport; and (III) toxicological effects. For example, AgNPs can be released from textiles by simple washing (Benn and Westerhoff 2008; Geranio et al. 2009), while toxicology studies of pristine AgNPs suggest the potential for DNA damage to mammalian cells as well as toxicity to microbes, insects, and fish (Pal et al. 2007; Ahamed et al. 2008; Choi and Hu 2008; Rai et al. 2009; Demir et al. 2010; Kim et al. 2010b).

One of the major issues for nanoparticle-related ecotoxicological studies, however, is a lack of mechanistic and kinetic information on the transformations of specific engineered nanoparticle (ENP) properties caused by environmental and industrial factors (Klaine et al. 2008). Such transformations can make accurately predicting the persistence of nanomaterials difficult, therefore hindering detailed life-cycle analyses. Identifying transformation products and quantifying transformation rates is needed to (1) provide a focus for the limited resources available for toxicity testing, and (2) determine the potential hazards posed by ENPs released into the environment. Several studies have advanced our knowledge of AgNPs' transformation, fate, and transport in the environment. For example, recent reports indicate that AgNPs may transport great distances from their point of origin in rivers (Kennedy et al. 2010), partially agglomerate and settle into soils depending upon aquatic conditions (e.g., water hardness and natural organic matter) (Chinnapongse et al. 2011) or rapidly transform into silver sulfide nanoparticles in wastewater treatment plants (Kim et al. 2010a). Oxidation and dissolution of AgNP suspensions in the absence of light can also occur and proceed at a rate dependent upon pH and dissolved oxygen (DO) content (Liu and Hurt 2010), with kinetics that depend on surface coatings and available surface area (Liu et al. 2010). Dissolution resulting in greater Ag^+ concentrations has also been shown under environmentally relevant (Akaighe et al. 2011) conditions.

The light-induced transformation of AgNPs is a topic that has only been briefly explored to date. UV light in the 260–400 nm wavelength range (equivalent to the UVA and UVB ranges) can modify 3 nm AgNPs by causing their surface plasmon resonance (SPR) to decrease, at a rate which increases with the photon energy (Linnert et al. 1991). The SPR loss was attributed to AgNP dissolution into Ag^+, with the dissolution rate dependent upon solution conditions and the presence of reactive oxygen species (ROS) scavengers. In contrast, AgNP suspensions stabilized with polymeric coatings (e.g., polyvinyl pyrrolidone and gum Arabic) aggregate in the presence of sunlight (Cheng et al. 2011). While these studies and others have advanced our knowledge, it is clear that more information is needed on how the physical properties of AgNPs suspensions, such as size and stabilizer concentration, impact transformation products, and degradation rates in the presence of light.

Therefore, the focus of the current study is on the light-induced transformation rates and products of differently sized, citrate-capped AgNP suspensions. For irradiation, a UV lamp with a wavelength intensity distribution centered at 300 nm was used, representing the greater energy portion of the solar spectrum. Changes to the size, optoelectronic properties, and stability of the suspended AgNPs were measured as a function of UV exposure, size, and concentration of the citrate stabilizer. Evidence for AgNP oxidation, dissolution, and morphological transformations was found, and both quantitative and qualitative data on the photophysical and photochemical transformations that may occur to AgNP suspensions in aqueous conditions will be presented.

Experimental

Materials and sample preparation[1]

Citrate-capped AgNPs (henceforth referred to as AgNPs) of the NanoXact product line were purchased from Nanocomposix (San Diego, CA) in a phosphate buffer with nominal particle diameters of (20, 40, 60, and 80) nm and a silver concentration of 20 mg L^{-1}.

[1] Certain trade names and company products are mentioned in the text or identified in illustrations in order to specify adequately the experimental procedure and equipment used. In no case does such identification imply recommendation or endorsement by National Institute of Standards and Technology, nor does it imply that the products are necessarily the best available for the purpose.

The manufacture states only trace levels of citrate remain in solution. To compare the effects of UV irradiation on citrate-capped AgNPs from a second source, 20 nm AgNPs were synthesized "in-house" using well-established protocols (see Supporting Information (SI)) (Chinnapongse et al. 2011; Zook et al. 2011a; MacCuspie et al. 2011a). Silver nitrate, trisodium citrate, and sodium borohydride ($NaBH_4$) (Part Numbers 209139, S1804, and 452882, respectively, Sigma Aldrich, St. Louis, MO) were used as received without further purification. All AgNP suspensions were diluted using milli-Q water ($\approx$18.2 MΩ) to a concentration of (4, 6 or 10) mg L^{-1} for photolysis experiments with an unadjusted pH range of (7.5–7.9) and a DO content of $\approx$6.0–8.0 mg L^{-1} (DO content was measured prior to exposure with an Extech DO700 meter). All AgNP suspensions were kept at room temperature in the dark until used, typically within 1 week.

The impact of trisodium citrate concentration on the rate of AgNP photolysis was studied with the 20-nm in-house synthesized particles. Since these AgNP suspensions (60 mg L^{-1}) were stored at greater citrate levels (49.2 mg L^{-1}) relative to the silver concentration, the suspensions were adjusted to lower citrate concentrations by centrifugation prior to analysis. Briefly, a volume of the stock suspension was centrifuged at $\approx$10,000$\times g$ for over 40 min to form an AgNP pellet at the base of the tube. Subsequently, a volume of supernatant was removed to decrease the citrate concentration to the desired level (ranging from 0.88 to 36.08 mg L^{-1}). Lastly, the pellet was re-suspended and adjusted to attain the desired working AgNP concentration with 1 mmol L^{-1} sodium phosphate. All AgNP suspensions were UV-exposed less than 24 h after completion of the aforementioned procedure. In other photolysis experiments following a similar procedure for citrate removal, the AgNP suspensions were typically prepared at lower citrate concentrations for ease of comparing to the Nanocomposix (commercial) suspensions.

UV light source

Reactor specifications

UV irradiation of AgNP suspensions was performed using a Rayonet mini-reactor (RMR-600) from Southern New England Ultraviolet (Branford, CT). The Rayonet reactor consists of eight UV-emitting bulbs with an emission wavelength centered at $\approx$300 nm (range 250–350 nm; full width half max of approximately 35 nm, estimated from manufacturer's data) with a carousel stage that rotates for uniform UV exposure. The reactor also comes equipped with a cooling fan to prevent sample heating during UV exposure. Quartz vials (RQV-7, Southern New England Ultraviolet, Branford, CT) were filled to less than 50 % capacity (6–7 mL) with AgNP stock suspensions, sealed with parafilm, and placed in a radially symmetric arrangement on the carousel stage to ensure uniform exposure. For kinetic studies, the light source was turned off at the desired time points; the quartz tubes were removed and wrapped in foil to block the light until analysis by UV–vis (typically within 24 h of exposure). Each sample placed in the Rayonet was exposed once to irradiation, analyzed and then discarded. Control studies were performed using 20 nm AgNP suspensions with the vials shielded by aluminum foil. All experiments (unless otherwise stated) were carried out with all eight bulbs operating with a total irradiance of 47.38 W/m^2. An experiment to determine the effect of light intensity on transformation kinetics was performed by reducing the number of bulbs in a radially symmetric fashion.

Measurement of total photon flux

To provide a basis for comparisons with future studies, the photon flux and fluence rate were measured using potassium ferrioxalate actinometry, consistent with well-established literature methods (Hatchard and Parker 1956). Specifically, 2 mL of 6.8 mmol L^{-1} ferrioxalate (in 0.1 mol L^{-1} H_2SO_4) was irradiated for a given time; the photolyzed samples were subsequently mixed with 2 mL of 1,10 phenanthroline (6.1 mol L^{-1}) (L) and 1 mL of 0.6 mol L^{-1} sodium acetate buffer (in 0.36 mol L^{-1} H_2SO_4) and then diluted to a final volume of 20 mL with DI water. After irradiation, a new absorption band developed at 510 nm, indicating the formation of a photochemically reduced Fe(II)L complex. The absorbance at 510 nm increased linearly as a function of irradiation time with a gradient of 1.66×10^{-2} s^{-1}. Using equations from the literature, this approach was used to determine that the photon flux was $\approx 2.18 \times 10^{16}$ photons s^{-1} with all eight bulbs operating, which was used for all experiments except the irradiance study (Nic et al. 2006; Braslavsky 2007). To estimate the photon fluence rate or irradiance, the

photon flux is divided by the cross-sectional area of the quartz vial (inner diameter × height ≈ 3.05 cm^2) used for actinometry, with the assumption that the photon flux is uniform throughout the entire suspension. This calculation yielded a value of 7.15×10^{15} photons s^{-1} cm^{-2}, or 47.38 W m^{-2} (assuming all photons are at a wavelength of 300 nm) (Nic et al. 2006; Braslavsky 2007; Björn 2008).

Instrumentation

UV–visible spectroscopy

AgNP suspensions were analyzed using two different UV–vis spectrophotometers. A Perkin Elmer (Waltham, MA) Lambda-9000 UV–Vis (double beam) spectrophotometer was employed for the majority of the studies. A Shimadzu (Columbia, MD) UV-1800 UV Spectrophotometer (double pass) was employed to determine the impact of citrate concentration on the photolysis rate and in experiments involving the 60-nm AgNPs. In each case, measurements were made using a quartz cuvette with a one cm path length. For kinetic measurements, changes in the absorbance at the peak SPR wavelength (λ_{max}) of a non-exposed AgNP sample were used. A spectrum of a blank water sample was used for background subtraction.

Atomic force microscopy (AFM)

The AFM methodology followed recommendations outlined in the NIST-Nanotechnology Characterization Laboratory (NIST-NCL) assay cascade protocol PCC-6 (Grobelny et al. 2009). AFM samples were deposited within 24 h of UV exposure onto 3-aminopropyldimethylethoxysilane-functionalized (Gelest, Morrisville, PA) polished Si substrates. A 20-μL drop of the irradiated AgNP suspension (4–6 mg L^{-1}) was allowed to sit for 30 min on the substrate, rinsed with filtered DI water and dried with short blasts of compressed, filtered air. This methodology prevents agglomeration due to drying or sample processing (Grobelny et al. 2009; Geronimo and MacCuspie 2011). Immobilized AgNPs prepared in this way were stored in particle-free cabinets, and analyzed within 4 weeks. AFM measurements were performed using a Bruker AXS (Santa Barbara, CA) Dimension 3100 with a Nanoscope V controller operating in intermittent contact mode. Cantilevers with nominal spring constants of 7.4 N m^{-1} (NanoAndMore, Lady's Island, SC) and a reported tip radius of curvature <8 nm were used to collect all images. Particle size histograms were constructed using Nanoscope software (v. 7.20b, Bruxer AXS, Santa Barbara, CA) from no less than 100 measurements of individual AgNPs per sample, and confirmed with automated image analysis (Boyd and Cuenat 2011). Results are reported as the mean size of all nanoparticles measured, with an uncertainty of one standard deviation about the mean. This uncertainty represents the polydispersity or the width of the size distribution.

Dynamic light scattering (DLS)

The DLS methodology followed recommendations outlined in the NIST-NCL assay cascade protocol PCC-1 (Hackley and Clogston 2007). DLS measurements were performed using a Malvern Instruments (Westborough, MA) Zetasizer Nano in 173° backscatter mode. All samples were prepared in a particle-free hood. Disposable semi-micro cuvettes (BrandTech Scientific, Inc., Essex, CT) were cleaned with filtered compressed air. Photolyzed AgNPs were analyzed at (20.0 ± 0.1) °C within 24 h of UV exposure. The cumulants analysis algorithm was applied to obtain the Z_{avg} equivalent hydrodynamic diameter and the polydispersity index (PI). Results reported are the mean and one standard deviation based on five measurements of each sample. Note, this uncertainty represents the repeatability of the measurement, rather than the width of the size distribution (MacCuspie et al. 2011b).

Liquid flow-cell transmission electron microscopy (TEM)

Liquid, flow-cell TEM imaging, or liquid TEM, was carried out in a specialized specimen holder (Poseidon™) using microfluidic chips manufactured by Protochips, Inc. (Raleigh, NC). In this technique, the nanoparticle suspension was contained within a microfluidic cell, which consisted of two silicon microfluidic chips. Each chip had an electron transparent silicon nitride (SiN_x) window 50 nm thick with a 30 μm × 30 μm lateral viewing area. The samples prepared for liquid TEM were 20 nm, in-house AgNP suspensions ([Ag] = 4 mg L^{-1}) prepared with a greater citrate concentration (49.2 mg L^{-1}), both with and without shielding from ≈5,300 min of UV

exposure. The reason a greater citrate concentration was employed was to ensure that the AgNPs did not aggregate with each other or absorb to the fluidic lines. To prepare the AgNPs for imaging, a 0.75-μL droplet of stock solution was deposited between two microchips and closed together. The microfluidic cell was then loaded into the vacuum-tight TEM holder without drying. The microfluidic cell interfaced with the holder to provides fluid circulation from outside of the electron microscope, maintaining constant hydration (Ring and de Jonge 2010; Klein et al. 2011).

Bright-field images were acquired with incident energy $E_0 = 300$ keV, collection angle $\beta = 5.4$ mrad and an energy-selecting slit of width $\Delta E = 10$ eV. TEM images were processed such that the grayscale intensities were autoscaled to maximize the dynamic range. Size analysis of AgNPs was performed manually with individual size measurements for the unexposed AgNPs. Due to the asymmetry of the exposed AgNPs, two measurements were made for each particle along the longest and the shortest dimensions. These diameters were combined into average particle diameters and standard deviations are representative of >80 individual measurements. Average shell thickness is representative of >20 individual particle measurements at greater resolution.

X-ray photoelectron spectroscopy (XPS)

To perform XPS on the unexposed AgNPs, 2 vials containing 1.5 mL of 20 nm in-house synthesized AgNP suspensions (4 mg L^{-1}) were centrifuged ($\approx 10{,}000 \times g$) for ≈ 10 min. From each vial, the pellet was deposited (<0.1 mL) in series onto a cleaned silicon wafer. Prior to UV exposure, these same AgNP suspensions were prepurified to contain 0.88 mg L^{-1} citrate. Once these AgNPs were irradiated for $\approx 2{,}500$ min, the same procedure was performed to prepare samples for XPS, although in the absence of a clearly visible pellet a <0.1 mL drop was deposited from the bottom of the centrifuge vial. Once deposited, both unexposed and UV-exposed AgNPs were mounted onto a sample bar for introductory pumping and analyzed at a base pressure of 2.66×10^{-7} Pa.

XP spectral acquisition was performed on a Kratos Axis Ultra DLD spectrometer (Chestnut Ridge, NY) equipped with a monochromated Al Kα source (1486.6 eV) and a low energy electron source for charge neutralization. Full spectra were acquired using a pass energy of 160 eV (1.0 eV/step) to determine the identity of all elements present; multiplexes of specific regions including the Ag $3d^{5/2}$ photoelectron peak and Ag MNN Auger transitions were taken at a pass energy of 40 eV (0.1 eV/step). Analysis of XPS data was performed using CasaXPS software (Casa Software Ltd, Teignmouth, UK) with the raw spectra fit to a Shirley background and all binding energies adjusted to the C (1s) peak at 284.5 eV (Molder et al. 1992). To estimate the Auger transition maximum, the Ag MNN spectra was fit with five Gaussian peaks. The fit of the Auger electron profile is merely meant as a guide to the eye. For ease of visualization and comparison, the individual spectra were background subtracted and normalized to a common peak height. Control samples for modified Auger parameter measurements were performed on silver(I) oxide powder (Sigma Aldrich # 221163, St. Louis MO) and silver metal foil (National Physics Laboratory, Middlesex, UK).

Donnan membrane technique (DMT) and inductively coupled plasma-mass spectrometry (ICP-MS)

The DMT cells, as originally described by Temminghoff et al. (2000), were used to quantify Ag^+ concentrations in pristine and UV-exposed AgNP suspensions based on theory, modeling, and applications which have been thoroughly discussed elsewhere (Weng et al. 2005, 2010; Kalis et al. 2006, 2007). Additionally, a schematic representation (SI Figure S1) as well as more details on the experimental protocol can be found in the SI.

In brief, a cation exchange membrane (551652U, CTL Scientific Supply Corp., Deer Park, NY) was used to separate a donor solution (containing both AgNPs and ions) from an acceptor solution. These membranes were cleaned and conditioned by successively shaking with solutions of 0.1 mol L^{-1} HNO_3, (milli-Q), 1 mol L^{-1} $Ca(NO_3)_2$, (in milli-Q water) and 0.1 mmol L^{-1} $Ca(NO_3)_2$ prior to use. The donor solution consisted of either 0.1 mg L^{-1} of Ag^+ prepared by adding an appropriate mass of $AgNO_3$, or 0.1 mg L^{-1} citrate-capped AgNPs (exposed or unexposed). The pH of donor and acceptor solutions was 5.3 ± 0.2 (average and standard deviation based on 20 measurements) and the solutions were kept at room temperature throughout the entire experiment. To generate a sufficient mass of photolyzed 20 nm AgNPs to perform replicates at 0.1 mg L^{-1}, a

significantly greater concentration of nanoparticles were UV-exposed. Specifically, in-house synthesized, AgNP suspensions at 10 mg L^{-1} with a lesser relative citrate concentration (16.4 mg L^{-1}) were prepared and irradiated for approximately 7,000 min. After irradiation, the suspensions were immediately diluted into the donor solutions for analysis.

During the DMT analysis, both donor and acceptor solutions were constantly circulated through the small volume of the cell where active cation exchange occurs at 2.5 mL min^{-1} (see SI Figure S1B). At specific intervals (including prior to initiating the experiment), 2 mL samples were taken from both the donor and acceptor solutions. To quantify the transfer and equilibration of Ag^{+} to steady state concentrations, removed samples from both the donor and the acceptor were quantified with ICP-MS using EPA method 200.8/6020.

Results

Particle size and citrate concentration dependent kinetics

Irradiation of the 20 nm AgNPs (in-house synthesized and commercial) for ≈8,000 min caused the suspension to change from the characteristic yellow color of the AgNPs to a near colorless solution, while control suspensions shielded from the light over the same time period produced no color change (Fig. 1). There were no visibly observable indications of sedimentation, aggregation, agglomeration, or plating post irradiation. UV–vis spectroscopy was therefore employed to determine the kinetics of the color change by recording the SPR intensity as a function of exposure time.

In Fig. 2, absorbance spectra are shown for (20, 40, 60, and 80) nm AgNP suspensions after various irradiation times (t_{exp}). The SPR absorbance maxima (λ_{max}) at $t_{exp} = 0$ were observed at (402, 412, 432 and 455) nm for the (20, 40, 60 and 80) nm AgNPs, respectively. For all AgNPs, the SPR absorption at λ_{max} decreased as t_{exp} increased. For 20 nm AgNPs, ≈95 % of the initial absorbance at λ_{max} was lost after $t_{exp} \approx$ 7,000 min, an effect observed in both commercial and "in-house" sources of 20 nm AgNP suspensions. For comparable exposure times and larger particle sizes, however, a greater percentage of the initial λ_{max} absorbance remained, decreasing by less than 50 % for 80 nm AgNPs. Thus, the magnitude of SPR absorbance loss increased as the AgNP diameter decreased (Fig. 2).

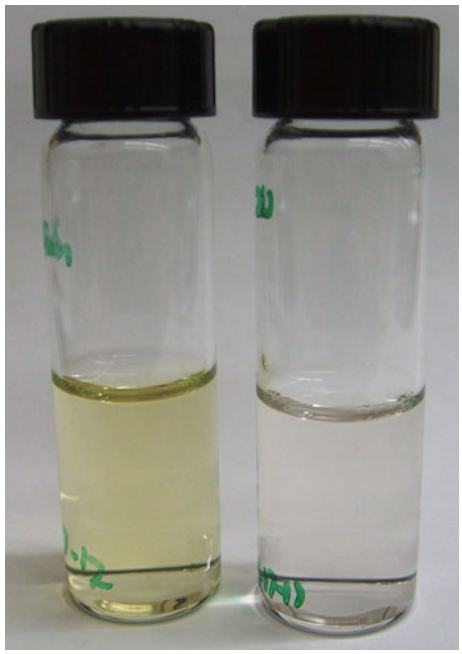

Fig. 1 Effect of 300 nm irradiation on 20 nm AgNP suspensions (4.0 mg L^{-1}, commercial). Unexposed control suspension retained the characteristic *yellow color* (*left*) while exposed samples (≈8,000 min) became near colorless (*right*). (Color figure online)

Additionally, λ_{max} blue-shifted steadily throughout exposure for most AgNP suspensions indicating a decrease in the particle diameter. The largest blue-shifts were for the larger AgNPs, such as (60 and 80) nm, which shifted approximately 15 nm to shorter wavelengths at $t_{exp} \approx$ 7,000 min. Occasionally, irradiation was accompanied by the appearance of a new absorbance peak or broadening in the absorption spectrum between 500 and 650 nm, as illustrated in the 20 nm (t_{exp} = 1,100 min) and 40 nm (t_{exp} = 5,734 min) AgNPs (Fig. 2). Such behavior was not evident in the larger diameter AgNPs. This increase in absorbance intensity at longer wavelengths (producing a bi-modal spectra) also has been reported in pulsed laser studies on AgNPs and attributed to the formation of larger NPs through either particle aggregation or fusion (Popov et al. 2006; Duan et al. 2009) as well as evidence for silver nanoprisms (Xue et al. 2008). This is also similar to the SPR coupling observed with clusters and agglomerates of gold nanoparticles (Tsai et al. 2011; Zook et al. 2011c).

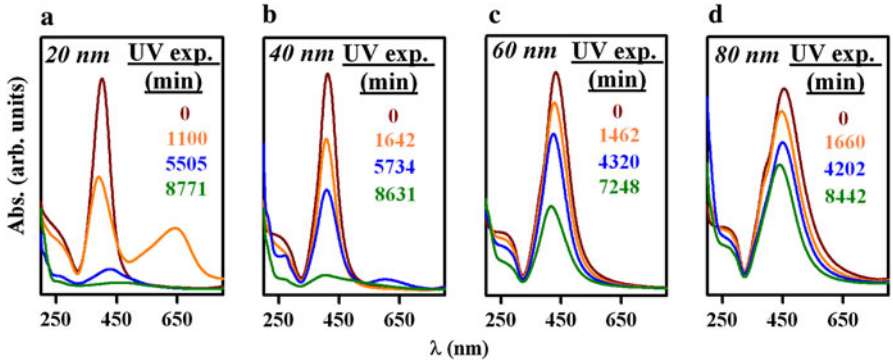

Fig. 2 Absorbance spectra of 20, 40, 60 and 80 nm (6.0 mg L^{-1} in **a** and 4.0 mg L^{-1} in **b–d**, respectively) commercial AgNPs after different exposures to 300 nm light. In all cases, SPR absorbance decreases with increasing exposure time (single measurements)

Figure 3a shows the normalized change in SPR absorbance (A_t/A_0), measured at λ_{max}, and plotted as a function of t_{exp}. For each AgNP diameter, A_t/A_0 could be fit to an exponential decay, indicative of a pseudo-first-order kinetic process. In Fig. 3b, the pseudo-first-order rate constants (k_{obs}) extracted from Fig. 3a were plotted versus the specific surface area (SSA), or a measure of the total surface area (cm^2) per gram of AgNPs in suspension. The k_{obs} uncertainty is the standard error of the exponential fit from Fig. 3a, and the SSA was calculated based on the AFM measured average diameter of the initial particles (Table 1). The plot of k_{obs} versus SSA was linear ($R^2 = 0.98$), indicating that photo-reactivity is directly proportional to the SSA of the pristine AgNPs. To verify that UV exposure was the cause of these absorbance changes, a light-shielded control experiment was performed which resulted in no measurable transformation to the physico-chemical properties of the AgNPs (SI Figure S2).

The effect of UV light intensity was examined using 20 nm AgNPs exposed for a constant time with a k_{obs} representative of the SPR loss at a given irradiance. Results demonstrated the pseudo-first-order rate constant had a non-linear dependence on irradiance (SI Figure S3), suggesting a process mediated by multi-photon absorption. While a power law fit ($k_{obs} = a \times I^n$) indicated an approximately 7 photon process, based on the limited number of irradiance values tested this should only be considered an estimate.

The impact of citrate concentration on the photolysis of "in-house" AgNP suspensions was also studied (Fig. 4). At the greatest citrate concentration (36.08 mg L^{-1}), these 4.0 mg L^{-1} AgNP suspensions (Fig. 4a) decreased by $\approx$50 % in SPR absorbance intensity when exposed to UV radiation ($t_{exp} \approx$ 2,500 min). Additionally, a slight shift and broadening towards longer wavelengths was observed. A comparison of the data shown in Fig. 4 shows that the degree of SPR loss increased as the citrate concentrations decreased. Thus, at 6.56 mg L^{-1} citrate concentrations, the SPR loss was >95 % and at 0.88 mg L^{-1} the SPR absorbance was below the detection limit.

Transformations to the AgNP diameter and morphology

AFM and DLS were used to determine how UV exposure affected the size distribution of the commercial AgNPs. Figure 5a–d depicts representative AFM images of unexposed AgNPs acquired from stock commercial suspensions prior to irradiation. Based on the analysis of over 100 particles, height histograms were generated for each type of AgNP (Fig. 5e–h). The unexposed AgNPs were predominantly monodispersed with mean heights and standard deviation of (20.1 ± 3.6), (37.0 ± 12.9), (61.9 ± 6.8), and (77.4 ± 24.1) nm for the nominal diameters of (20, 40, 60 and 80) nm, respectively (Table 1). All AgNP mean diameters measured by DLS (Table 1, SI Figure S4) also increased systematically for the different sizes, but were consistently larger than the AFM measurements, as expected from previous studies (MacCuspie et al. 2011b). Figure 5e–h shows the AFM size distributions for all diameters of AgNPs after prolonged UV exposure ($t_{exp} \approx$ 8,000 min). The particle height histograms support the hypothesis that UV exposure leads to a decrease in average particle size. AgNPs with (20 and 40) nm nominal diameters decreased to (13.2 ± 18.1) and (20.7 ± 12.7) nm, respectively, after irradiation (Table 1). Similarly, the mean heights measured for the 60 and 80 nm nominal diameter AgNPs decreased upon irradiation to (11.9 ± 13.4) and (11.0 ± 12.6) nm, respectively.

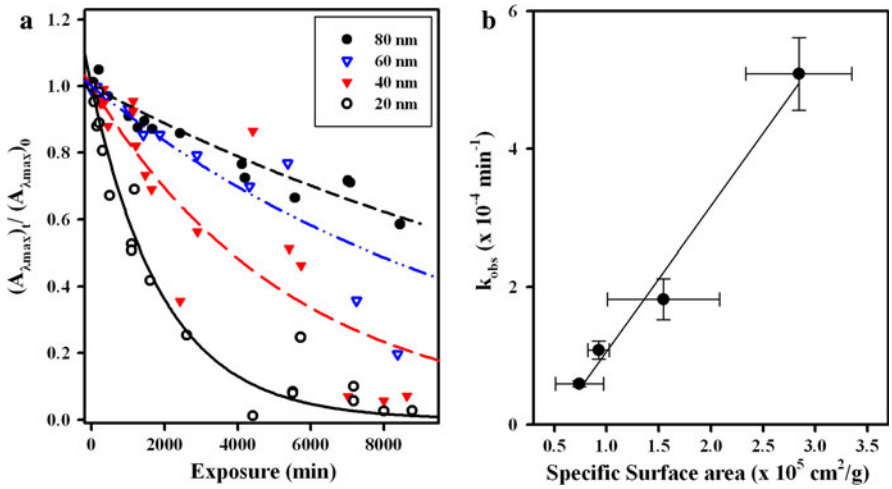

Fig. 3 **a** Normalized SPR absorbance, $(A_{\lambda max})_t/(A_{\lambda max})_0$, versus light exposure for AgNP suspensions (same conditions as Fig. 2) are plotted and fit to a pseudo-first-order kinetic process (coefficient of determination (r^2) > 0.90 for 20 and 80 nm AgNPs; $r^2 > 0.80$ for 40 and 60 nm). **b** The k_{obs} values plotted versus the AgNP's specific surface area (calculated from AFM average particle diameter). The *vertical error bars* represent the error of the exponential decay fit and *horizontal error bars* are propagated from the AFM standard deviation. The fit was linearly correlated with an $r^2 > 0.98$

Table 1 AFM and DLS measurements for (20, 40, 60, and 80) nm AgNPs (4.0 mg L^{-1}, commercial), both exposed and shielded. The means and polydispersity index (PI) for the DLS measurement is derived from five consecutive measurements of one sample under the same conditions, while the standard deviation for each AFM measurement is derived from >100 individual particle height measurements

UV light exposure (min)	Nominal AgNP diam. (nm)	AFM mean diam. (nm)	SD (nm)	DLS mean *Z*-average diam. (nm)	Polydispersity index (PI)
$t = 0$	20	20.1	3.6	30.4	0.270
$t = 8{,}771$	20	13.2	18.1	144.2	0.121
$t = 0$	40	37.0	12.9	42.2	0.205
$t = 8{,}631$	40	20.7	12.7	24.7	0.535
$t = 0$	60	61.9	6.8	64.81	0.106
$t \approx 8{,}000$	60	11.9	13.4	45.24	0.216
$t = 0$	80	77.4	24.1	86.8	0.064
$t \approx 8{,}000$	80	11.0	12.6	72.5	0.136

DLS measurements also confirmed that the AgNP diameters decreased after irradiation, with the exception of the 20 nm AgNPs (Table 1, SI Figure S4), which will be discussed later.

Liquid TEM was performed on the in-house synthesized, 20 nm AgNPs (4 mg L^{-1}) for samples before and after UV exposure (≈5,300 min) (Fig. 6), which resulted in >80 % SPR loss and some broadening (SI Figure S5). As previously mentioned, the AgNPs were suspended in 49.2 mg L^{-1} citrate (Fig. 4a) to prevent excessive particle aggregation and deposition onto the flow cell. The unexposed AgNPs (Fig. 6a, b) demonstrated uniform, monodisperse, spherical particle characteristics with a measured diameter of (20.2 ± 3.1) nm. After UV exposure, the AgNPs became increasingly asymmetric with a decreased particle size of (13.9 ± 3.7) nm as measured across the longest dimension. Most notably, the presence of an outer layer, or 'shell', approximately (2.7 ± 0.8) nm thick developed (Fig. 6c, d). Additionally, the asymmetry of the particle cores suggests that multiple particles aggregated and fused together.

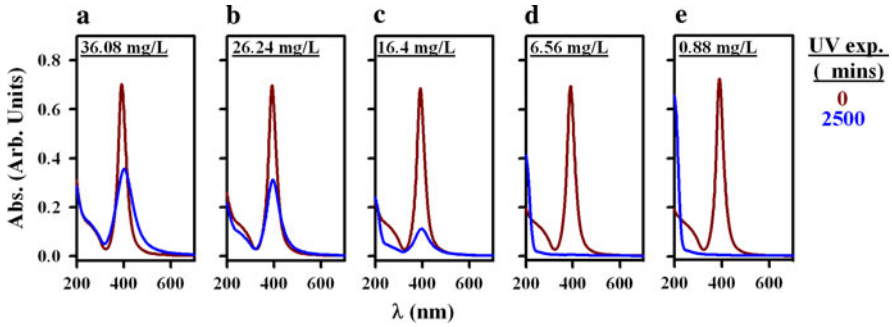

Fig. 4 Citrate concentration dependence on the rate of 20 nm AgNP (4.0 mg L^{-1}) photolysis after approximately 2 days of UV exposure. The citrate concentration is indicated in the *top left hand corner* of each plot. At greater citrate concentrations (36.08 mg L^{-1}) the degree of SPR loss was the smallest and was accompanied by a substantial broadening of the SPR band. At the lowest citrate concentrations (0.88 mg L^{-1}), the SPR intensity was completely removed by photolysis

Some larger (>50 nm in diameter) AgNP aggregates were also observed.

Chemical transformations

XPS analysis was used to identify the surface chemical transformations associated with the UV exposure of in-house synthesized 4 mg L^{-1}, 20 nm AgNP suspensions under the smallest relative citrate concentration (0.88 mg L^{-1}) in 0.1 mmol L^{-1} phosphate (same conditions as Fig. 4d). Lesser citrate concentrations were explored due to the faster rate of loss of the SPR as observed with the in-house synthesized particles (Fig. 4d) and the commercial AgNPs (Fig. 5) with "trace" citrate levels. Figure 7 compares the photoelectrons detected from the unexposed AgNPs to those observed after the suspension had been UV-exposed for ≈2,550 min. As displayed in Fig. 7, the Ag $3d^{5/2}$ XPS transition and the Ag Auger MNN peak were collected. The photoelectrons were plotted versus binding energy (BE) while the Auger MNN electrons were plotted versus kinetic energy (KE). To extract chemical information on the oxidation state of silver, modified Auger parameters (α') were calculated using the following equation (Briggs and Seah 1990):

$$\alpha' = \mathrm{BE}_{\mathrm{Ag\,3d5/2}} + \mathrm{KE}_{\mathrm{Ag\,MNN}}$$

For Ag, determining α' is the best way to analyze the oxidation state for silver using XPS due to a relatively minor shift in the Ag ($3d^{5/2}$) BE (<1.0 eV) for most of silver's potential oxidation products, a shift that can be obscured by minor charging phenomena (Wagner 1975; Wagner et al. 1979; Molder et al. 1992). In contrast, modified Auger parameters for Ag are more sensitive to changes in oxidation state and moreover are not influenced by charging because they are internally determined within a given spectrum. Prior to photolysis, α' was 726.1 eV which is consistent with both literature values and measurements made on a sputter cleaned silver foil. After photolysis, α' shifted to 724.4 eV, comparable with reference values for Ag_2O of 724.5 eV (Schon 1973; Briggs and Seah 1990) and within 0.2 eV of an Ag_2O reference sample (724.2 eV).

Wet chemical tests for oxidized silver were also performed using qualitative techniques. Specifically, commercial (Fig. 8a) and in-house (Fig. 8b) suspensions of 20 nm AgNPs (4 mg L^{-1}) were UV-exposed for t_{exp} ≈ 2,500 min. Lesser relative citrate concentrations were selected for the in-house AgNP suspensions to approximate the trace citrate levels in the commercial samples. After UV exposure, absorbance measurements were acquired and confirmed the complete loss of the SPR in both suspensions. Subsequently, $NaBH_4$ (a strong reducing agent) was added to the suspensions, and the characteristic absorbance and yellow coloration reappeared. The $NaBH_4$-induced reduction of oxidized silver species in the UV-exposed suspensions resulted in metallic AgNPs. However, this result does not elucidate whether multiple oxidation products are present.

DMT was used to differentiate between the Ag^+ and AgNP fractions. DMT analysis results can be graphically represented as a ratio of the metal concentration in the acceptor (the ionic portion) to the total metal concentration in the donor ($Ag_{acceptor}$/Ag_{donor}). For example, when this ratio equals 0.5 upon reaching equilibrium, 50 % of the total metal in the

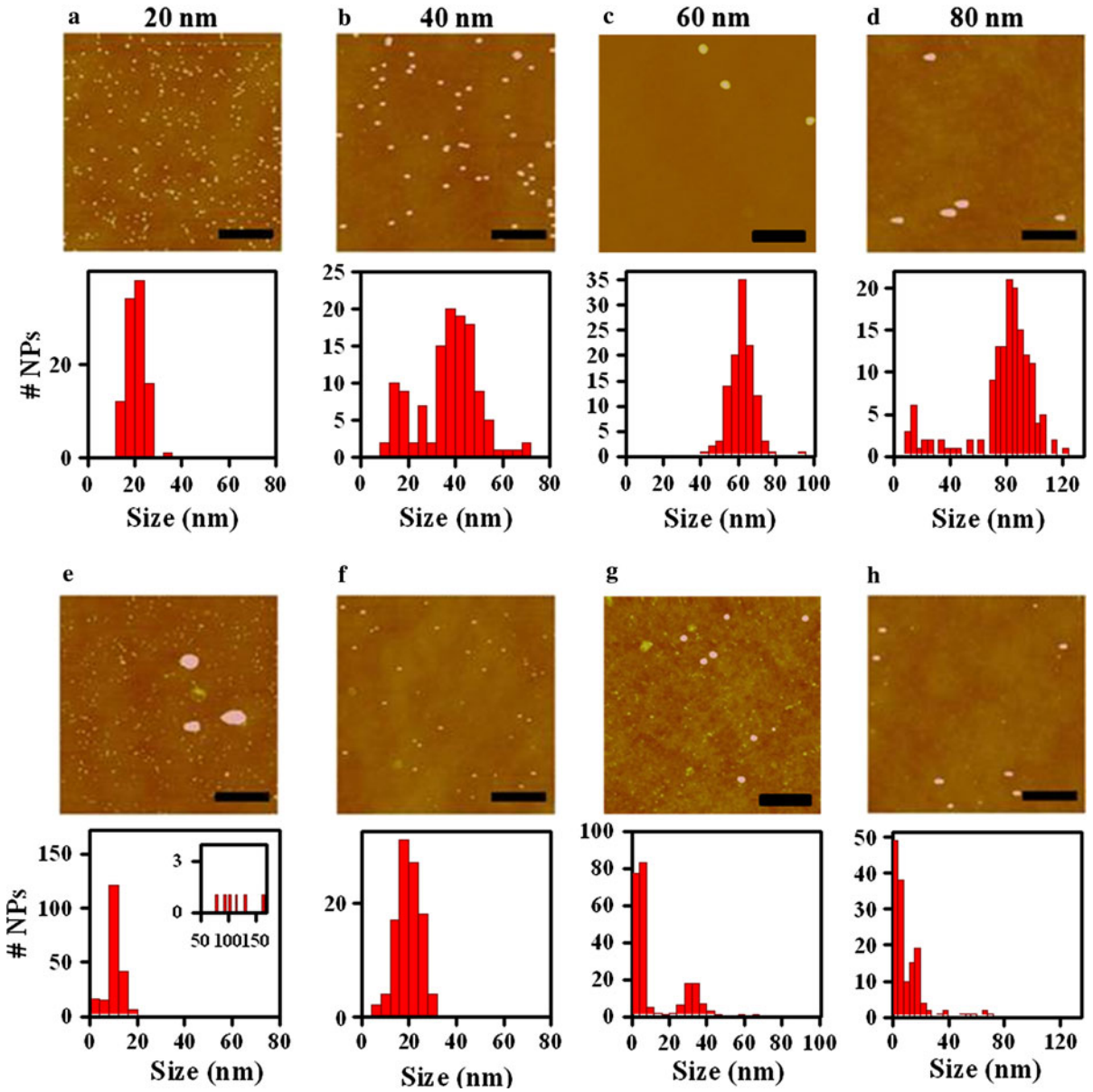

Fig. 5 Representative AFM images and corresponding histograms depict the size change for each AgNP suspension (4.0 mg L^{-1}, commercial) **a–d** before and **e–h** after UV exposure ($t_{exp} \approx$ 8,000 min). Length *scale bars* are 500 nm for all AFM images. For the UV-exposed 20-nm AgNPs the *inset* shows the small number of larger structures present, likely aggregated AgNPs

donor solution would be considered in the ionic form. The $AgNO_3$ control solution achieved equivalent Ag concentrations in the acceptor and donor solutions ($Ag_{acceptor}/Ag_{donor} = 1.0$) after 48 h (Fig. 9), confirming the DMT's ability to transfer Ag ions completely. The equilibration rates of the AgNP suspensions, however, were dictated by UV exposure. UV-exposed AgNPs reached equilibrium in approximately 70 h, with approximately 76 % of the total Ag concentration in the ionic form, corresponding closely to the $AgNO_3$ rate. By comparison, pristine AgNPs reached equilibrium after a much longer time (>200 h) and had a lower fraction of Ag^+ ($Ag_{acceptor}/Ag_{donor} = 0.54$).

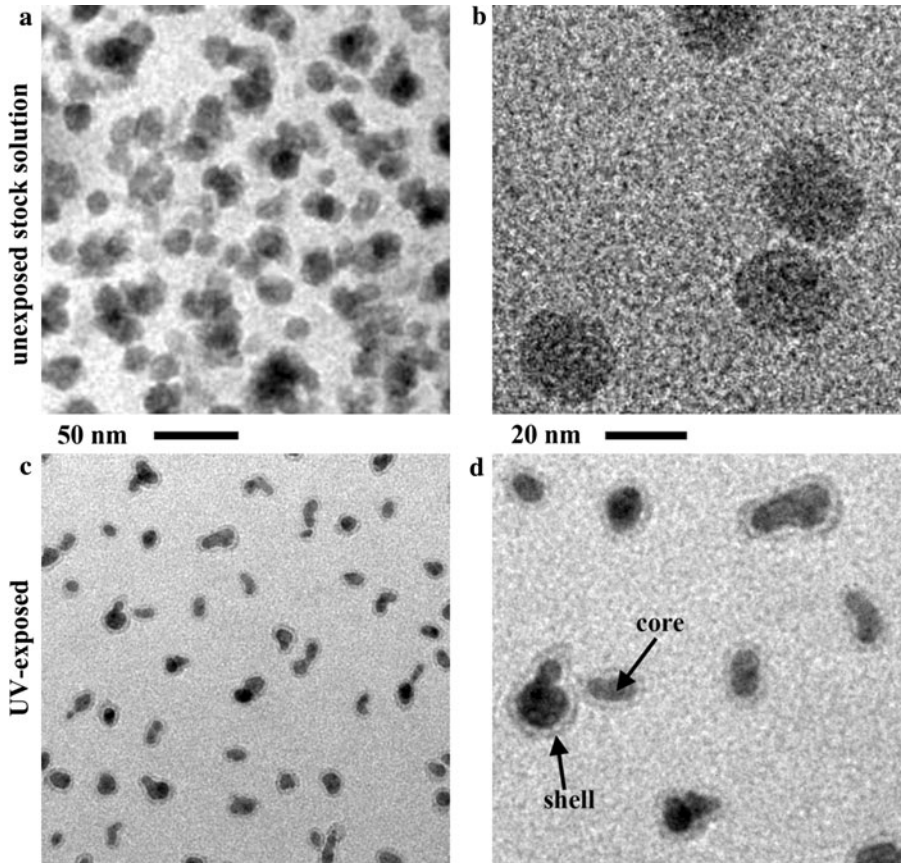

Fig. 6 In situ liquid TEM images of the 20-nm AgNP suspension (4.0 mg L^{-1}) stabilized with greater citrate (48.68 mg L^{-1}) before (**a**, **b**) and after (**c**, **d**) UV exposure for 4 days. *Scale bar* for **a**, **c** 50 nm and **b**, **d** 20 nm

Discussion

The effect of UV radiation on AgNP suspensions resulted in transformations to the individual particles and new products which were detected over the course of this study. The loss of the SPR absorbance (Fig. 2) suggests that these transformations are surface dependent, as demonstrated by the linear correlation associated with the linear correlation for the AgNPs rate of degradation as related to the SSA (Fig. 3b) and the inhibiting effect of increased citrate stabilizer (Fig. 4). A loss or alteration in the SPR absorbance has been observed in previous AgNP studies and has been attributed to the following potential transformations: a surface layer formed as a result of Ag oxidation (e.g., Ag_2O, Ag_2S, Ag_3(citrate)) could alter optical properties dependent upon the structure of the shell (Pradhan et al. 2001), complete conversion into an Ag_2O NP through oxygen diffusion (Thomas et al. 2008), and/or conversion to Ag^+, a phenomena observed in other light-shielded dissolution studies (Liu and Hurt 2010; Liu et al. 2010). From the observations in the current study, UV exposure causes citrate-capped AgNP suspensions to transform into physico-chemical states that include contributions from both oxidation and physical transformations products, as summarized in Fig. 10.

Surface oxidation of the citrate-capped AgNPs is one of the consequences of UV exposure and provides a succinct explanation for the observations in this study (Fig. 10). Perhaps the clearest evidence for surface oxidation was observed from the TEM images (Fig. 6c, d) where the irradiated 20 nm AgNPs decreased in diameter and developed a shell 2.7 nm $\pm$ 0.8 nm thick. This uniformly lighter gray shell exhibited significantly less contrast than the dark core, suggesting a different material at the particle's surface with decreased mass-density (ρ) compared to

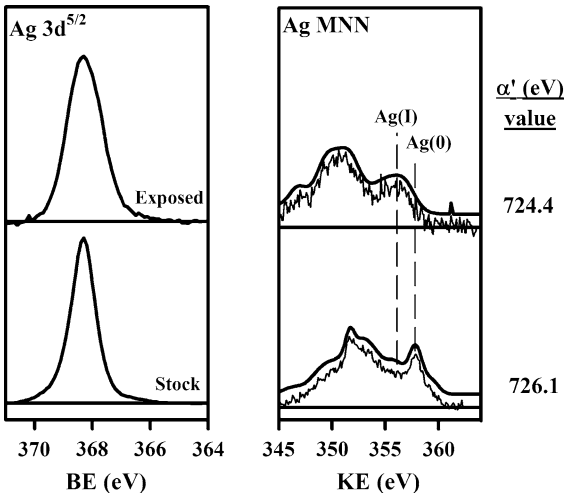

Fig. 7 XPS analysis of lesser relative citrate concentration (0.88 mg L^{-1}), 20 nm AgNP suspensions (4.0 mg L^{-1}) synthesized in-house, before and after UV exposure ≈2,500 min. In the exposed AgNP suspensions, the Auger parameter (α') decreased suggesting an increase in silver oxidation

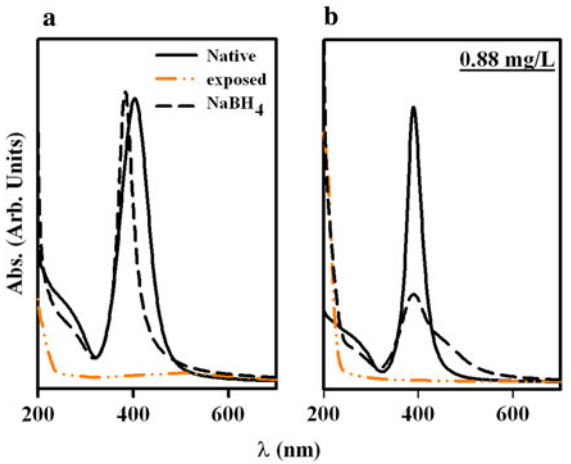

Fig. 8 $NaBH_4$ reduction of the UV-exposed 20 nm. **a** AgNPs suspension (4.0 mg L^{-1}, commercial) and **b** 4.0 mg L^{-1}, in-house synthesized AgNP suspensions at a 0.88 mg L^{-1} citrate. The SPR peak was restored for both materials, confirming a photooxidation process had occurred

metallic silver. The core material also showed signs of diffraction contrast (Fig. 6a, b). XPS measurements (Fig. 7) revealed a shift in the α' to a value indicative of Ag_2O, suggesting that the shell observed in the TEM images resulted from transformation of metallic silver into silver (I) oxide ($\rho_{Ag_2O} = 7.14$ g cm^{-3} versus $\rho_{Ag(0)} = 10.49$ g cm^{-3}) (Lide 1999). This would explain why a large number of smaller particles

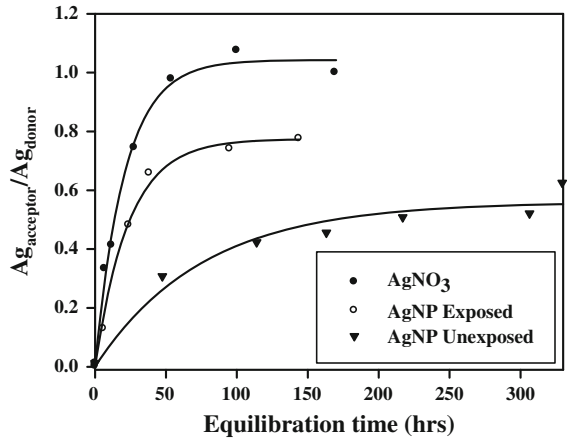

Fig. 9 Donnan membrane measurements of UV-exposed (≈7,000 min) and shielded AgNP suspensions (diluted to 0.1 mg L^{-1} and exposed at 10 mg L^{-1}) with a lesser relative citrate (0.1622 and 16.22 mg L^{-1}, respectively) concentrations. For reference, silver nitrate sample is also shown. UV-exposed AgNP suspensions exhibit a sharp increase in silver ion transferred to the acceptor solution, comparable to the rate for silver nitrate. Shielded AgNP suspensions have a slower transfer rate, suggestive of dissolution upon dilution, which is an artifact of the DMT technique

were observed by multiple techniques (AFM, liquid TEM) even after the absorbance measurements for the SPR had decreased by >95 %. For example, while 13.2 nm metallic AgNPs (AFM measured average diameter for photolyzed 20 nm AgNPs, Table 1) should still possess an SPR absorbance, a sufficiently thick shell of oxidized silver could eliminate the SPR.

For irradiated samples, the observation of an oxidized layer on the surface of the UV-exposed AgNPs offers a potential route for dissolution to occur, because silver oxide has been noted to be water soluble, with a solubility product constant of 0.026 mg/L (Klosky and Woo 1926; Lide 1999) which would be sufficiently large to dissolve the AgNPs in suspension. Direct evidence for the presence of Ag^+ was found from the DMT experiment shown in Fig. 9. These measurements suggested that not all of the Ag in the oxidized AgNPs dissolved to Ag^+, consistent with the persistence of small nanoparticles at comparable UV exposures. It should be noted that unexposed AgNP suspensions also exhibited a slow rise to a non-zero equilibrium value. This observation can be attributed to dissolution through dilution as has been observed in other recent studies (Liu and Hurt 2010). In contrast, UV–vis and DLS showed that unexposed AgNPs showed no loss of SPR intensity or

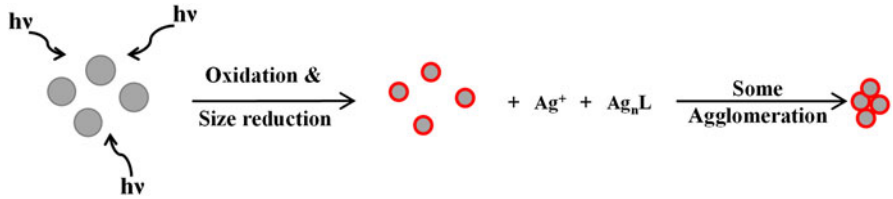

Fig. 10 Illustration of the proposed mechanism of photoinduced transformations of AgNPs when exposed to 300 nm UV light. Oxidation of the AgNP surface is followed by dissolution into silver cations and a subsequent decrease in particle size, and some agglomeration or aggregation. ● pristine AgNP, ◯ surface-oxidized AgNP, *n* number of atoms, *L* ligand

change in particle size, supporting the idea that the Ag^+ released in the DMT experiments is a consequence of the dilution needed to perform these particular studies. Thus, some of the Ag^+ produced from the irradiated AgNP samples and observed by the DMT in Fig. 9 may be attributed to this dilution effect, but the shorter time to equilibrium and the greater equilibrium ratio in the UV-exposed suspensions suggests that increased concentrations of Ag^+ were present initially. Moreover, an oxidation process which produces either Ag^+ or oxidized AgNPs would allow for the recovery of the SPR from UV-exposed AgNPs upon addition of a reducing agent such as $NaBH_4$ (Fig. 8), a test successfully performed on multiple different UV-exposed AgNP suspensions as well as a proven technique from the literature (Pradhan et al. 2001).

A logical conclusion to draw from the evidence for AgNP dissolution is that the release of Ag^+ would ultimately result in a decrease in the average particle diameter, as was been observed in AFM, TEM and DLS analysis (Figs. 5, 6; Table 1, SI Figure S4). The one exception was the irradiated 20 nm AgNP suspensions, which revealed a particle size increase by DLS. This is likely the result of a few large aggregates forming in the suspensions and the underlying metrology employed. A small number of aggregates were observed by AFM, and transiently by UV–vis absorbance. However, the volume-squared-weighted DLS measurement disproportionately increases the average particle diameter reported. For 20 nm AgNP suspensions, the average particle diameters (with standard deviations) decreased to (13.2 ± 18.1) and (13.9 ± 3.7) nm based on AFM and TEM measurements, respectively.

Aggregation of the AgNP suspensions after UV irradiation was also observed in select spectra. Specifically, particle aggregation was observed in certain absorbance spectra (Fig. 2), AFM images (Fig. 5b), and DLS results (Table 1) for 20 and 40 nm AgNPs. The detected absorbance increase at (500–700 nm) is consistent with previous observations of small clusters or agglomerates of AgNPs (Cheng et al. 2011; Zook et al. 2011b). Insufficient citrate concentrations may provide one explanation for the observed aggregation of smaller AgNPs upon UV exposure. Specifically, decreasing the AgNP diameter via photolysis would result in an overall increase in SSA, and, if the citrate concentration remained constant through the experiment, there could be insufficient stabilizer present to inhibit aggregation. This could also explain why the smaller-diameter AgNPs (20 and 40 nm) were the suspensions more prone to aggregation since the citrate concentration in solution for the size-dependent study (Fig. 2) was reported by the manufacturer as constant across AgNP diameters. Another route to aggregation could be due to insoluble surface films on the AgNPs, which could lead to poor interactions with the citrate stabilizer, resulting in decreased colloidal stability; however this would be expected to affect all sizes of AgNPs. Lastly, it is important to mention the potential for the citrate itself to transform, as has been reported previously, which could also result in decreased colloidal stability (Xue et al. 2008; Jiang et al. 2010).

An alternate pathway for photo-induced size reduction could involve AgNP fragmentation, which was originally reported in pulsed laser studies (Kamat et al. 1998; Kamat 2002). However, while fragmentation and surface deformation processes have been demonstrated experimentally with short bursts of extremely large fluence rates and theoretically may be possible with extremely long exposures at low fluence rates (Dai et al. 2011), there is insufficient data to either confirm or deny whether this process occurs in this study. Surface oxidation followed by dissolution, however, is also consistent with the size-dependent kinetics which ultimately resulted in a rate dependent

upon the SSA (Fig. 3b). The reduction in photolysis rate from increased citrate concentration (Fig. 4) also supports this since an increase in the stabilizer concentration would presumably block surface sites for oxidation and/or dissolution, resulting in a decreased rate of removal of the outer layers of the AgNP. Considered collectively, the data and the literature suggest that SPR loss accompanied by size reduction can be caused by multiple different transformation pathways. From the observations in the current study, multiple transformations, including Ag oxidation and dissolution, occurred. This photochemical process has been found to depend upon the SSA of the suspensions and, consistently, is partially inhibited by the presence of excess citrate.

The transformative effects of UV radiation on citrate stabilized AgNP suspensions have been demonstrated to be a surface oxidation process resulting in dissolution and size reduction. From a nanoEHS risk assessment perspective, the most likely point during the life-cycle of AgNPs for UV exposure to play a role will be after their release from materials into the natural waterways where solar exposure becomes a possibility. Many investigations into aqueous AgNP suspensions (typically in the absence of light) have demonstrated that a combination of oxidation, such as sulfidation and dissolution, aggregation and/or persistence of single nanoparticles can occur when environmentally and biologically relevant solution conditions are varied (e.g., salinity, pH, O_2, O_3, ROS, HS, and natural macromolecules) (Liu and Hurt 2010; Liu et al. 2010; Levard et al. 2011, 2012; Stebounova et al. 2011; MacCuspie 2011). Additionally, other studies have demonstrated the existence of a residual fraction of single particles which remain suspended in the natural waterways (Chinnapongse et al. 2011; Zook et al. 2011a; Piccapietra et al. 2012). The results from the current study suggest that if released into natural waterways, individually suspended AgNPs are likely to be impacted by photochemical and photophysical transformations due to solar exposure in surface and near surface waters.

Conclusions

The UV-induced physico-chemical transformations to AgNP suspensions have been presented. Transformation products include surface oxidation of AgNPs resulting in a core–shell structure, dissolution into Ag^+, and agglomeration/aggregation. The UV-induced loss of the SPR and decrease in AgNP diameter has been demonstrated to be dependent upon the (1) SSA (diameter) of AgNPs and (2) concentration of excess citrate present in the solution phase of the suspension. While the photodegradation of citrate-capped AgNP suspensions is likely to result in some physico-chemical transformations, the specific change has been demonstrated to be dependent upon both particle and solution phase conditions.

Acknowledgments The authors acknowledge the National Research Council for funding and Ben Yezer for useful comments and suggestions. The cleaning, membrane conditioning, and sampling protocols were kindly supplied by Dr. Erwin Temminghoff (Wageningen University). DHF acknowledges support from an NIEHS SEED grant administered by JHU School of Public Health.

References

Ahamed M, Karns M et al (2008) DNA damage response to different surface chemistry of silver nanoparticles in mammalian cells. Toxicol Appl Pharmacol 233(3): 404–410

Akaighe N, MacCuspie RI et al (2011) Humic acid-induced silver nanoparticle formation under environmentally relevant conditions. Environ Sci Technol 45(9):3895–3901

Benn TM, Westerhoff P (2008) Nanoparticle silver released into water from commercially available sock fabrics. Environ Sci Technol 42:4133–4139

Björn LO (2008) Principles and nomenclature for the quantification of light. In: Björn LO (ed) Photobiology. Springer, New York, pp 41–49

Boyd RD, Cuenat A (2011) New analysis procedure for fast and reliable size measurement of nanoparticles from atomic force microscopy images. J Nanopart Res 13(1):105–113

Braslavsky SE (2007) Glossary of terms used in photochemistry, 3rd edition (IUPAC Recommendations 2006). Pure Appl Chem 79(3):293–465

Briggs D, Seah MP (1990) Practical surface analysis. Wiley, Chichester

Cheng Y, Yin L et al (2011) Toxicity reduction of polymer-stabilized silver nanoparticles by sunlight. J Phys Chem C 115(11):4425–4432

Chinnapongse SL, MacCuspie RI et al (2011) Persistence of singly dispersed silver nanoparticles in natural freshwaters, synthetic seawater, and simulated estuarine waters. Sci Total Environ 409(12):2443–2450

Choi O, Hu Z (2008) Size dependent and reactive oxygen species related nanosilver toxicity to nitrifying bacteria. Environ Sci Technol 42:4583–4588

Costanza J, El Badawy AM et al (2011) Comment on "120 years of nanosilver history: implications for policy makers". Environ Sci Technol 45(17):7591–7592

Dai Y, He M et al (2011) Femtosecond laser nanostructuring of silver film. Appl Phys A 106(3):567–574

Demir E, Vales G et al (2010) Genotoxic analysis of silver nanoparticles in Drosophila. Nanotoxicology. doi:10.3109/17435390.2010.529176

Duan JS, Park K et al (2009) Optical properties of rodlike metallic nanostructures: insight from theory and experiment. J Phys Chem C 113(35):15524–15532

Geranio L, Heuberger M et al (2009) The behavior of silver nanotextiles during washing. Environ Sci Technol 43(21): 8113–8118

Geronimo CLA, MacCuspie RI (2011) Antibody-mediated self-limiting self-assembly for quantitative analysis of nanoparticle surfaces by atomic force microscopy. Microsc Microanal 17(2):206–214

Grobelny J, DelRio FW et al (2009) NIST-NCL Joint Assay Protocol PCC-6: size measurements of nanoparticles using atomic force microscopy. NIST, Gaithersburg, MD

Hackley VA, Clogston JD (2007) NIST-NCL Joint Assay Protocol PCC-1: measuring the size of nanoparticles in aqueous media using batch-mode dynamic light scattering. NIST, Gaithersburg, MD

Hatchard CG, Parker CA (1956) A new sensitive chemical actinometer. 2. Potassium ferrioxalate as a standard chemical actinometer. Proc R Soc Lond Ser A-Math Phys Sci 235(1203):518–536

Jiang XC, Chen CY et al (2010) Role of citric acid in the formation of silver nanoplates through a synergistic reduction approach. Langmuir 26(6):4400–4408

Kalis EJJ, Weng LP et al (2006) Measuring free metal ion concentrations in situ in natural waters using the Donnan Membrane Technique. Environ Sci Technol 40(3): 955–961

Kalis EJJ, Weng LP et al (2007) Measuring free metal ion concentrations in multicomponent solutions using the Donnan membrane technique. Anal Chem 79(4):1555–1563

Kamat PV (2002) Photophysical, photochemical and photocatalytic aspects of metal nanoparticles. J Phys Chem B 106: 7729–7744

Kamat PV, Flumiani M et al (1998) Picosecond dynamics of silver nanoclusters. Photoejection of electrons and fragmentation. J Phys Chem B 102:3123–3128

Kennedy AJ, Hull MS et al (2010) Fractionating nanosilver: importance for determining toxicity to aquatic test organisms. Environ Sci Technol 44(24):9571–9577

Kim B, Park C-S et al (2010a) Discovery and characterization of silver sulfide nanoparticles in final sewage sludge products. Environ Sci Technol 44(19):7509–7514

Kim J, Kim S et al (2010b) Differentiation of the toxicities of silver nanoparticles and silver ions to the Japanese medaka (*Oryzias latipes*) and the cladoceran *Daphnia magna*. Nanotoxicology. doi:10.3109/17435390.2010.508137

Klaine SJ, Alvarez PJJ et al (2008) Nanomaterials in the environment: behavior, fate, bioavailability, and effects. Environ Toxicol Chem 27(9):1825–1851

Klein KL, Anderson IM et al (2011) Transmission electron microscopy with a liquid flow cell. J Microsc 242(2):117–123

Klosky S, Woo L (1926) Solubility of silver oxide in mixture of water and alcohol. J Phys Chem 30(9):1179–1180

Levard Cm, Reinsch BC et al (2011) Sulfidation processes of PVP-coated silver nanoparticles in aqueous solution: impact on dissolution rate. Environ Sci Technol 45(12): 5260–5266

Levard C, Hotze EM et al (2012) Environmental transformations of silver nanoparticles: impact on stability and toxicity. Environ Sci Technol 46:6900–6914

Lide DR (1999) Handbook of chemistry and physics. Chemical Rubber Pub. Co., Cleveland

Linnert T, Mulvaney P et al (1991) Photochemistry of colloidal silver particles—the effects of N_2O and adsorbed CN^-. Ber Bunsen Phys Chem 95(7):838–841

Liu J, Hurt RH (2010) Ion release kinetics and particle persistence in aqueous nano-silver colloids. Environ Sci Technol 44:2169–2175

Liu J, Sonshine DA et al (2010) Controlled release of biologically active silver from nanosilver surfaces. ACS Nano 4(11):6903–6913

MacCuspie RI (2011) Colloidal stability of silver nanoparticles in biologically relevant conditions. J Nanopart Res 13(7): 2893–2908

MacCuspie RI, Allen AJ et al (2011a) Dispersion stabilization of silver nanoparticles in synthetic lung fluid studied under in situ conditions. Nanotoxicology 5(2):140–156

MacCuspie RI, Rogers K et al (2011b) Challenges for physical characterization of silver nanoparticles under pristine and environmentally relevant conditions. J Environ Monit 13(5):1212–1226

Maynard A (2010) Project on emerging nanotechnologies. Woodrow Wilson International Center for Scholars. http://www.nanotechproject.org/inventories/consumer/analysis_draft/

Molder JF, Stickle WF et al (1992) Handbook of X-ray photoelectron spectroscopy. Perkin-Elmer Corporation, Eden Prairie

Nic M, Jirat J et al (2006) IUPAC. Compendium of chemical terminology (the "Gold Book"), 2nd ed. Blackwell Scientific Publications, Oxford. http://goldbook.iupac.org. ISBN 0-9678550-9-8. doi:10.1351/goldbook

Nowack B (2010) Nanosilver revisited downstream. Science 330(6007):1054–1055

Nowack B, Krug HF et al (2011a) Reply to comments on "120 years of nanosilver history: implications for policy makers". Environ Sci Technol 45(17):7593–7595

Nowack B, Krug HF et al (2011b) 120 Years of nanosilver history: implications for policy makers. Environ Sci Technol 45(4):1177–1183

Pal S, Tak YK et al (2007) Does the antibacterial activity of silver nanoparticles depend on the shape of the nanoparticle? A study of the gram-negative bacterium *Escherichia coli*. Appl Environ Microbiol 73(6):1712–1720

Piccapietra F, Sigg L et al (2012) Colloidal stability of carbonate-coated silver nanoparticles in synthetic and natural freshwater. Environ Sci Technol 46(2):818–825

Popov AK, Brummer J et al (2006) Synthesis of isolated silver nanoparticles and their aggregates manipulated by light. Laser Phys Lett 3(11):546–552

Pradhan N, Pal A et al (2001) Catalytic reduction of aromatic nitro compounds by coinage metal nanoparticles. Langmuir 17(5):1800–1802

Rai M, Yadav A et al (2009) Silver nanoparticles as a new generation of antimicrobials. Biotechnol Adv 27(1):76–83

Ring EA, de Jonge N (2010) Microfluidic system for transmission electron microscopy. Microsc Microanal 16(05):622–629

Schon G (1973) ESCA studies of Ag, Ag_2O and AgO. Acta Chem Scand 27(7):2623–2633

Stebounova LV, Guio E et al (2011) Silver nanoparticles in simulated biological media: a study of aggregation, sedimentation, and dissolution. J Nanopart Res 13(1):233–244

Temminghoff EJM, Plette ACC et al (2000) Determination of the chemical speciation of trace metals in aqueous systems by the Wageningen Donnan Membrane Technique. Anal Chim Acta 417(2):149–157

Thomas S, Nair SK et al (2008) Size-dependent surface plasmon resonance in silver silica nanocomposites. Nanotechnology 19:075710. doi:10.1088/0957-4484/19/7/075710

Tolaymat TM, El Badawy AM et al (2010) An evidence-based environmental perspective of manufactured silver nanoparticle in syntheses and applications: a systematic review and critical appraisal of peer-reviewed scientific papers. Sci Total Environ 408(5):999–1006

Tsai DH, Cho TJ et al (2011) Hydrodynamic fractionation of finite size gold nanoparticle clusters. J Am Chem Soc 133(23):8884–8887

Wagner CD (1975) Chemical shifts of Auger lines, and the Auger parameter. Faraday Discuss Chem Soc 60:291

Wagner CD, Gale LH et al (1979) 2-Dimensional chemical-state plots—standardized data set for use in identifying chemical-states by X-ray photoelectron-spectroscopy. Anal Chem 51(4):466–482

Weng LP, Van Riemsdijk WH et al (2005) Kinetic aspects of donnan membrane technique for measuring free trace cation concentration. Anal Chem 77(9):2852–2861

Weng LP, Van Riemsdijk WH et al (2010) Effects of lability of metal complex on free ion measurement using DMT. Environ Sci Technol 44(7):2529–2534

Wiesner MR, Lowry GV et al (2009) Decreasing uncertainties in assessing environmental exposure, risk and ecological implications of nanomaterials. Environ Sci Technol 43: 6458–6462

Xue C, Métraux GS et al (2008) Mechanistic study of photomediated triangular silver nanoprism growth. J Am Chem Soc 130(26):8337–8344

Zook JM, Long SE et al (2011a) Measuring silver nanoparticle dissolution in complex biological and environmental matrices using UV–visible absorbance. Anal Bioanal Chem 401(6):1993–2002

Zook JM, MacCuspie RI et al (2011b) Stable nanoparticle aggregates/agglomerates of different sizes and the effect of their size on hemolytic cytotoxicity. Nanotoxicology 5(4): 517–530

Zook JM, Rastogi V et al (2011c) Measuring agglomerate size distribution and dependence of localized surface plasmon resonance absorbance on gold nanoparticle agglomerate size using analytical ultracentrifugation. ACS Nano 5(10): 8070–8079